Cation ordering in Pb²⁺-bearing, Mn³⁺-rich pargasite from Långban, Sweden

Ulf Hålenius[1],* and Ferdinando Bosi[2,3]

[1]Department of Mineralogy, Swedish Museum of Natural History, Box 50007, SE-10405 Stockholm, Sweden
[2]Dipartimento di Scienze della Terra, Sapienza Università di Roma, P.le A. Moro, 5, I-00185 Rome, Italy
[3]CNR-IGG Istituto di Geoscienze e Georisorse, Sede di Roma, P.le A. Moro, 5, I-00185 Roma, Italy

Abstract

A multi-analytical approach using electron microprobe analysis, X-ray structural refinement, and polarized single-crystal Fourier transform infrared spectroscopy was used to characterize short-range and long-range structures of a Pb²⁺-bearing, Mn³⁺-rich pargasite. Site populations, derived from the results of site-scattering refinement and stereochemical analysis, demonstrate that Pb²⁺ is strongly ordered at the A-site in the monoclinic $C2/m$ amphibole structure. This finding is in agreement with the observed ordering of Pb²⁺ in the rare Pb²⁺-bearing $P2/a$ amphibole joesmithite, but is in contrast to a Pb²⁺ preference for the M4 site suggested by some studies on element partitioning between $C2/m$ amphiboles and melts. Mn³⁺ is strongly ordered at the M2 site in structure of the present amphibole. Contrasting results obtained for mean M2-O bond lengths and reported local Mn³⁺-O bond lengths as well as between bond-length distortion of the mean M2 polyhedron and the local Mn³⁺-centered M2O₆ octahedron in pargasite indicates that the structural relaxation of this polyhedron is complete or nearly so.

Keywords: Amphibole, pargasite, lead, manganese, structure refinement, IR spectroscopy

Introduction

The $C2/m$ symmetry is by far the most common structure-type in which amphibole supergroup minerals crystallize. The wide range of chemical compositions encountered in these amphiboles suggests that this is the most flexible of the six known amphibole structure-types.

In a recent report on an unusual Mn³⁺- and Pb-bearing pargasite from the famous Långban deposit (Jonsson and Hålenius 2010), it was suggested, on the basis of results obtained by optical absorption spectroscopy, that Mn³⁺ was ordered at the M2 site of the amphibole structure. This suggestion agrees with the observed strong ordering of trivalent transition metal cations at the M2 sites in the majority of clino-amphiboles (e.g., Ghose et al. 1986; Oberti et al. 1993). So far, the oxy-amphiboles ungarettiite, obertiite, and dellaventuraite with trivalent transition element cations ordering at M1 and M3 sites, represent the only observed exceptions to this ordering scheme (Hawthorne et al. 1995, 2000; Tait et al. 2005). Furthermore, Jonsson and Hålenius (2010) suggested, on the basis of optical absorption spectroscopy, that the local Mn³⁺-O distances at the M2 site are shorter and the degree of M2-O₆ polyhedral distortion is higher in pargasite than in magnesio-riebeckite and magnesio-arfvedsonite amphiboles (Ghose et al. 1986).

In the present work we have used X-ray single-crystal structure refinement and polarized single-crystal Fourier transform infrared (FTIR) spectroscopic techniques with the aim to evaluate the geometric characteristics of the cation polyhedra and cation ordering in this unusual amphibole. In addition to a special focus on the site distribution of the trivalent transition metal cations, a particular aim has been to define the occupancy of Pb²⁺. In

the very rare Pb- and Be-rich $P2/a$ amphibole joesmithite, $PbCa_2(Mg_3,Fe_2^{3+})(Si_6Be_2)O_{22}(OH)_2$, Pb²⁺ is ordered at the structural A site (Moore et al. 1993), but whether or not this ordering scheme is generally valid for all amphibole symmetries is not known. In most crystal-chemical studies, it is assumed that any small amounts of Pb²⁺ occasionally observed preferentially enters the A site, but some studies of element partitioning between melts and amphiboles argue that Pb²⁺ occupies the M4 site of the amphibole structure (e.g., Brenan et al. 1995). The present Pb²⁺-bearing pargasite provides an excellent opportunity to explore directly the Pb²⁺ distribution in a $C2/m$ amphibole.

Experimental methods

One selected gem quality, ca. $150 \times 200 \times 100$ μm, pargasite single crystal from the original specimen (NRM 20100001) described by Jonsson and Hålenius (2010) was used in the present investigation. The same crystal was studied by means of X-ray single-crystal diffraction, subsequently Fourier transform infrared spectroscopy in the OH stretching frequency range and finally chemical analysis by electron microprobe techniques.

Electron microprobe analysis

The chemical composition of the studied crystal was determined by means of electron microprobe techniques (EMP), using a Jeol JXA-8530F Hyperprobe equipped with four wavelength dispersive spectrometers and a field emission gun operated at 15 kV accelerating potential and 10 nA beam current at a beam diameter of 1 μm. Element standards used were albite (Na), orthoclase (K), Al_2O_3 (Al), $CaSiO_3$ (Ca and Si), MgO (Mg), $MnTiO_3$ (Mn and Ti), Fe_2O_3 (Fe), and vanadinite (Pb). Wavelength dispersive scans revealed no detectable amounts of any additional elements as, e.g., fluorine. The matrix corrections were performed according to the Armstrong-CITZAF method (Armstrong 1995). The amphibole formula was calculated assuming 46 negative charges per formula unit (Table 1).

X-ray structure refinement

X-ray diffraction measurements were performed at the Earth Sciences Department, Sapienza University of Rome, with a Bruker KAPPA APEX-II single-crystal diffractometer, equipped with CCD area detector (6.2×6.2 cm² active detection area, 512×512 pixels) and a graphite crystal monochromator, using Mo$K\alpha$ radiation

* E-mail: ulf.halenius@nrm.se

from a fine-focus sealed X-ray tube. The sample-to-detector distance was 4 cm. A total of 7980 exposures (step = 0.2°, time/step = 20 s) covering a full reciprocal sphere were collected. The orientation of the crystal lattice was determined from more than 500 strong reflections ($I > 100 \, \sigma_I$) evenly distributed in the reciprocal space, and used for subsequent integration of all recorded intensities. Final unit-cell parameters were refined by using Bruker AXS SAINT program from ca. 9909 recorded reflections with $I > 10 \, \sigma_I$ in the range $5 < °2\theta < 79$. The intensity data were processed and corrected for Lorentz, polarization, and background effects with the APEX2 software program of Bruker AXS. The data were corrected for absorption using a multi-scan method (SADABS). The absorption correction led to a significant improvement in R_{int}. No violation of $C2/m$ symmetry was noted.

Structure refinement was carried out with the SHELXL-97 program (Sheldrick 2008). Starting coordinates were taken from Oberti et al. (1995b). Variable parameters were: scale factor, extinction coefficient, atom coordinates, site-scattering values expressed as mean atomic number and atom displacement parameters. To obtain the best values of statistical indices ($R1$ and w$R2$) the oxygen sites were modeled with full-ionized oxygen scattering curves, while neutral curves were used for the cation sites. In detail, the A site was modeled using the Na scattering factor. The occupancies of the M1, M2, and M3 sites were refined considering the presence of Mg. The M4 and M4′ split sites were modeled by Ca and Mn, respectively. The T1 and T2 site were modeled with the Si scattering factor, but with unconstrained multiplicity for T1 and fixed occupancy of $Si_{1.00}$ for T2, because refinement with unconstrained multiplicity showed this latter site to be fully occupied by Si. Three cycles of full-matrix refinement with isotropic displacement parameters for all atoms were followed by anisotropic cycles until convergence was attained. Table 2 summarizes crystal data, data collection information and refinement details. Table 3 provides the refined atom coordinates and displacement parameters. Table 4 lists selected bond lengths and Table 5 gives mean atomic number (m.a.n.) at the cation sites in the structure. (A CIF[1] is available.)

Fourier transform infrared spectroscopy

Polarized $\mathbf{E}\|\alpha$ and $\mathbf{E}\|\gamma$ FTIR spectra were collected at room temperature in transmission mode in the spectral range 2000–5000 cm⁻¹ on a 46 µm thick doubly polished single crystal (010) slice during 256 cycles using a square-shaped ca. 60 ×60 µm aperture at a nominal spectral resolution of 2 cm⁻¹ with a Bruker Equinox 55S FTIR microscope spectrometer equipped with a KRS-5 polarizer, glowbar source, KBr beamsplitter, and MCT-detector. Recorded spectra were fitted using the peak resolution program Jandel PeakFit 4.0 assuming Gaussian lineshapes of equal widths and band positions constrained to those observed for OH stretching bands (labeled A–H) in unpolarized spectra of synthetic pargasite-dominant amphiboles along the richterite-pargasite join (Della Ventura et al. 1999).

TABLE 1. Electron microprobe analysis of pargasite NRM2010001

Spots analyzed; N=8	Mean	1σ
SiO₂ (wt%)	44.26	0.55
TiO₂	0.01	0.05
Al₂O₃	11.21	0.12
Mn₂O₃	3.56	0.16
Fe₂O₃	0.89	0.07
MgO	19.88	0.26
CaO	12.54	0.22
PbO	1.73	0.05
Na₂O	3.33	0.08
K₂O	0.18	0.03
H₂O_calc	2.09	
Sum	99.68	
Cations (apfu) on the basis of 46 negative charges		
Si	6.35	0.04
Ti	0.001	0.005
Al	1.90	0.02
Mn	0.39	0.02
Fe	0.10	0.01
Mg	4.25	0.05
Ca	1.93	0.03
Pb	0.067	0.006
Na	0.93	0.02
K	0.03	0.01

TABLE 2. Miscellaneous X-ray information

Crystal data	
Space group	$C2/m$
Z	2
a (Å)	9.9448(5)
b (Å)	18.0171(9)
c (Å)	5.2829(3)
β	105.445(2)
V (Å³)	912.39(8)
Crystal sizes (mm)	$0.12 \times 0.10 \times 0.05$
Data collection and refinement	
Radiation, Mo$K\alpha$ (Å)	0.71073
Temperature (K)	298(2)
Total number of frames	7980
Range for data collection, 2θ (°)	4.5 - 78.8
Reciprocal space range hkl	$-16 \le h \le 14$
	$-32 \le k \le 31$
	$-9 \le l \le 9$
Set of read reflections	23890
Unique reflections	2675
R_{int} (%)	1.72
Completeness (%)	99
Redundancy	8
Refinement method	Full-matrix least-squares on F^2
Extinction coefficient	0.0029(3)
w$R2$ (%)	5.99
$R1$ (%) all data	2.64
$R1$ (%) for $I > 2\sigma_I$	2.33
GooF	1.058

TABLE 3. Fractional atomic coordinates and equivalent (U_{eq}) or isotropic (U_{iso}) displacement parameters (Å²)

Atom	x	y	z	U^{11}	U^{22}	U^{33}	U^{23}	U^{13}	U^{12}	U_{eq}/U_{iso}*
O1	0.10767(7)	0.08634(4)	0.21947(13)	0.0078(3)	0.0108(2)	0.0084(2)	0.0002(2)	0.0017(2)	−0.0010(2)	0.0091(1)
O2	0.12024(7)	0.17250(4)	0.72790(12)	0.0057(3)	0.0091(2)	0.0079(2)	0.0003(2)	0.0014(2)	0.0002(2)	0.0076(1)
O3	0.10770(10)	0	0.71802(19)	0.0069(4)	0.0095(3)	0.0102(3)	0	0.0019(3)	0	0.0089(2)
O4	0.36588(8)	0.24907(4)	0.78694(13)	0.0115(3)	0.0085(2)	0.0109(2)	−0.0004(2)	0.0041(2)	−0.0026(2)	0.0101(1)
O5	0.34870(7)	0.13969(4)	0.11256(13)	0.0093(3)	0.0150(3)	0.0089(2)	0.0048(2)	0.0004(2)	−0.0004(2)	0.0114(1)
O6	0.34450(8)	0.11446(4)	0.61330(14)	0.0088(3)	0.0139(3)	0.0129(3)	−0.0051(2)	0.0029(2)	0.0008(2)	0.0118(1)
O7	0.34069(11)	0	0.2734(2)	0.0094(4)	0.0129(4)	0.0169(4)	0	0.0029(3)	0	0.0132(2)
T1	0.27974(3)	0.08489(1)	0.30315(5)	0.0066(1)	0.0071(1)	0.0071(1)	−0.00030(7)	0.00154(8)	−0.00048(7)	0.00699(7)
T2	0.28968(3)	0.17254(1)	0.81127(5)	0.0061(1)	0.00688(9)	0.00595(9)	0.00010(6)	0.00168(7)	−0.00047(7)	0.00629(6)
M1	0	0.08888(2)	1/2	0.0075(2)	0.0063(2)	0.0053(2)	0	0.0023(1)	0	0.0062(1)
M2	0	0.17595(2)	0	0.0056(2)	0.0051(2)	0.0049(2)	0	0.0018(1)	0	0.0051(2)
M3	0	0	0	0.0067(3)	0.0056(2)	0.0050(2)	0	0.0017(2)	0	0.0058(2)
M4	0	0.27952(3)	1/2	0.0113(1)	0.0074(2)	0.0101(1)	0	0.00564(8)	0	0.00906(7)
M4′	0	0.2628(8)	1/2							0.011(2)*
A2	0	0.47416(10)	0	0.0289(8)	0.048(1)	0.124(2)	0	0.038(1)	0	0.0639(6)
H3	0.210(3)	0	0.766(5)							0.013*

Note: H-atom was constrained to have a U_{iso} 1.5 times the U_{eq} value of the O3 oxygen.

TABLE 4. Selected bond distances (Å) in Pb²⁺-bearing, Mn³⁺-rich pargasite

Site-O		Site-O		Site-O	
T1-O1	1.6497(7)	T2-O4	1.5950(7)	A2-O7 × 2	2.4558(11)
T1-O7	1.6679(5)	T2-O2	1.6242(7)	A2-O5 × 2	2.7022(16)
T1-O6	1.6797(7)	T2-O5	1.6525(7)	A2-O6 × 2	2.7261(13)
T1-O5	1.6812(7)	T2-O6	1.6702(7)	A2-O6 × 2	3.3574(15)
<T1-O>	1.670	<T2-O>	1.635	A2-O5 × 2	3.4625(17)
Δ_{BS}	0.000057		0.000305	<A2-O>	2.941
σ^2	8.571		19.143		
<λ>	1.002		1.005		
M4-O4 × 2	2.3279(7)	M4'-O2 × 2	2.182(11)	A(2/m)-O7 × 2	2.4114(9)
M4-O2 × 2	2.4147(8)	M4'-O4 × 2	2.280(2)	A(2/m)-O6 × 4	3.0225(8)
M4-O6 × 2	2.6250(8)	M4'-O5 × 2	2.810(9)	A(2/m)-O5 × 4	3.0706(8)
M4-O5 × 2	2.6329(8)	M4'-O6 × 2	2.851(11)	<A(2/m)-O>	2.920
<M4-O>	2.500	<M4'-O>	2.531		
Δ_{BS}	0.002807		0.014262		
M1-O1 × 2	2.0469(7)	M2-O4 × 2	2.0176(7)		
M1-O3 × 2	2.0932(7)	M2-O2 × 2	2.1013(7)	M3-O3 × 2	2.0534(10)
M1-O2 × 2	2.0933(7)	M2-O1 × 2	2.1062(7)	M3-O1 × 4	2.0614(7)
<M1-O>	2.078	<M2-O>	2.075	<M3-O>	2.059
Δ_{BS}	0.000111		0.000383		0.000003
σ^2	39.65		23.03		54.84
<λ>	1.012		1.007		1.017

Notes: A(2/m) at (0, 1/2, 0).
Δ_{BS} = bond-length distortion according to Brown and Shannon (1973).
σ^2 = bond-angle variance according to Robinson et al. (1971).
<λ> = mean quadratic elongation according to Robinson et al. (1971).

RESULTS AND DISCUSSION

Chemical composition

The chemical composition of the studied pargasite crystal (Table 1) is very close to the one presented by Jonsson and Hålenius (2010). This suggests that chemical variations between individual crystals of pargasite in the present specimen are very limited. In addition, the present microprobe analyses (Table 1) confirm their observation that this Pb²⁺-bearing, Mn³⁺-rich pargasite is virtually free of fluorine. In accordance with the relationship between the M1-M2 distance and the *oxo* component in amphibole reported by Oberti et al. (2007), the occurrence of O²⁻ at the O3 site can also be ruled out as the observed M1-M2 distance equals 3.072 Å. The chemical composition of the present Pb²⁺-bearing, Mn³⁺-rich pargasite is fully consistent with ⁰³(OH) = 2 atoms per formula unit (apfu).

Site populations

The T1 and T2 sites. Although Si and Al have similar X-ray scattering factors (because of close atomic number Z = 14 and 13, respectively), the observed m.a.n. of the site T1 site is significantly smaller than 14, indicating the occurrence of a significant amount of Al in addition to Si (Table 5). This is also corroborated by the long observed <T1-O> distance, 1.670 Å (Hawthorne 1983). In contrast, the observed m.a.n. (14) and <T2-O> distance (1.635 Å) are fully consistent with a T2 site completely occupied by Si (e.g., Tait et al. 2001).

The M1, M2, and M3 sites. The observed m.a.n. at these sites are all significantly larger than 12, indicating that they are not only occupied by Mg (Z = 12) but also by heavier cations (Al³⁺, Mn³⁺, Fe³⁺ with Z = 13, 25, 26, respectively). To translate the crystal chemical and structural refinement results into site populations at M1, M2, and M3, experimental and calculated data from the atom distribution were optimized. By using a least-squares program and the ionic radii of Shannon (1976) the residuals between calculated and observed data (i.e., m.a.n. and

TABLE 5. Refined site-scattering values (expressed as m.a.n.) and site populations for Pb²⁺-bearing, Mn³⁺-rich pargasite

Site	Observed m.a.n.	Assigned site populations	Calculated m.a.n.	Calculated mean distance (Å)
T1	13.57(3)	$(2.37 \text{ Si} + 1.63 \text{ Al})_{\Sigma=4.00}$	13.59	1.678
T2	14	4.00 Si	14	1.625
M1	12.94(4)	$(1.82 \text{ Mg} + 0.11 \text{ Mn}^{3+} + 0.05 \text{ Fe}^{3+} + 0.02 \text{ Al})_{\Sigma=2.00}$	13.06	2.079
M2	13.76(4)	$(1.61 \text{ Mg} + 0.28 \text{ Mn}^{3+} + 0.11 \text{ Al})_{\Sigma=2.00}$	13.88	2.073
M3	12.71(5)	$(0.81 \text{ Mg} + 0.04 \text{ Mn}^{3+} + 0.14 \text{ Al})_{\Sigma=1.00}$	12.77	2.058
M4	19.32(4)	1.93 Ca	19.27	
M4'	0.85(5)	0.07 Mn²⁺	0.88	
Σ	20.17		20.15	
A2	15.9(1)	$(0.90 \text{ Na} + 0.067 \text{ Pb}^{2+})_{\Sigma=0.97}$	15.39	
A(m)		0.03 K	0.57	
Σ	15.9		15.96	

Note: m.a.n. = mean atomic number.

mean distances) were minimized. Final residuals are within the analytical uncertainties as shown by the comparison of data in Table 5. The results show that Mg is disordered over the M1, M2, and M3 sites with the highest population density at M1, whereas Al³⁺ and trivalent transition metal cations preferentially occupy M3 and M2 sites, respectively.

The M4 site. The <M4-O> distance of ~2.50 Å and the sum of m.a.n. at M4 + M4' of 20.2, indicates that this site is dominated by Ca (Z = 20). However, small amounts of cations with atom numbers higher than that of Ca must also be present (m.a.n. is over 20). Such cations may be related to the presence of a distinct M4' site (e.g., Oberti et al. 1993). In fact, during the structure refinement a significant residual peak (~0.5 e/Å³) was found in the residual electron density within the M4 cavity displaced along the twofold axis toward the M1 site. To dampen the high correlations that would otherwise occur between the refined M4 and M4' site variables, the displacement parameters of M4' were constrained to be isotropic. The refined position of M4' at (0, ~0.26, 1/2) and its related bond distances are fully consistent with the occurrence of Mn²⁺ in C2/m amphiboles (e.g., Oberti et al. 1993; Oberti and Ghose 1993; Oberti et al. 2006). As a result, Mn²⁺ was assigned to this site (Table 5). As the M4-M4' distance is shorter than the spatial resolution possible using X-ray data, the separation of m.a.n. at M4 and M4' could be affected by a large uncertainty. However, the occurrence of an amount of ca. 0.07 apfu (inferred as 2–1.93 Ca pfu) of Mn²⁺ at the M4' site seems to be compatible with the both the m.a.n. at M4' and analytical uncertainties of EMP measurements. It should also be noted that the suggested presence of a small fraction of Mn²⁺ within the M4 cavity is in agreement with the interpretation of the optical absorption spectra of this pargasite presented by Jonsson and Hålenius (2010).

The A site. It is well established that the A site in amphibole is affected by various locally ordered cation arrangements (e.g., Hawthorne et al. 1996). In the crystal studied a significant residual peak was found along the twofold axis. In fact, the residual electron density calculated from a difference-Fourier synthesis with the A-site cations removed from the refinement model showed a maximum at (0, 0.47, 0) with a significant electron density of about 15 e/Å³. Hence, the A2 site could be refined using anisotropic displacement parameters. The resulting residual electron densities, however, showed two remaining peaks at (0.03, 1/2, 0.05) and (0.01, 0.46, –0.04) with electron densities

TABLE 6. Bond-valence calculations (valence unit) for Pb^{2+}-bearing, Mn^{3+}-rich pargasite

Site	M1	M2	M3	M4	A	T1	T2	BVS
O1	0.39×2↓	0.33×2↓	0.37×4↓			0.96		2.05
O2	0.34×2↓	0.34×2↓		0.30×2↓			1.00	1.98
O3	0.34×2↓→		0.38×2↓					1.06
O4		0.42×2↓		0.37×2↓			1.08	1.88
O5				0.16×2↓	0.02×4↓	0.88	0.92	1.99
O6				0.17×2↓	0.03×4↓	0.87	0.88	1.96
O7					0.14×2↓	0.92×2→		1.97
BVS	2.15	2.19	2.22	2.02	0.47	3.64	3.88	

Note: BVS = bond-valence sums at the respective sites.

TABLE 7. Positions, widths, and areas of OH stretching bands in the present pargasite spectra

Polarization		**E‖α**		**E‖γ**	
Band	ν (cm⁻¹)	$w_{1/2}$ (cm⁻¹)	Relative area	$w_{1/2}$ (cm⁻¹)	Relative area
A	3731	20	0.039	22	0.017
B	3716	20	0.311	22	0.397
C	3705	20	0.171	22	0.115
D	3684	20	0.239	22	0.250
F	3672	20	0.142	22	0.090
G	3655	20	0.083	22	0.114
H	3640	20	0.015	22	0.018

Note: Estimated uncertainties for widths and relative areas of the bands are 1 cm⁻¹ and 0.008, respectively.

of about 1 e/Å³ at distances less than 0.6 Å from A2. The former peak can be explained by the ordering of small amounts of K at the A(*m*) site (e.g., Hawthorne et al. 1996), while the latter peak may be explained by ripples that normally are found close to heavy atoms (like Pb) at the end of a successful refinement. The refined site-scattering value at the A2 site (m.a.n. ~ 16) clearly shows that Pb^{2+} occurs in the A cavity. In fact, 0.9 apfu of Na (*Z* = 11) would yield a calculated m.a.n. at the A2 site that is too low (~9.9) and the observed site scattering (m.a.n. = 9.9 + 5.5 = 15.4) may only be explained by adding 0.067 apfu of Pb^{2+} (*Z* = 82). Site scattering information is also consistent with very small amounts of ^AK, and the EMP results (Table 1) are in accord with this inference. Finally, it is noteworthy that the studied amphibole is dominated (about 90%) by one of the most stable local arrangements indicated by bond-valence considerations for the amphibole structure (e.g., Hawthorne et al. 1996; Hawthorne and Harlow 2008): ^M4Ca-^O3OH-^A2Na.

In conclusion, although the relative large displacement parameters of A2 would suggest that a positional disorder involving more A-cations sites could occur, the studied amphibole results are described well by the presence of a dominant A2 site occupied by Na and Pb^{2+} along with likely very minor K at A(*m*). From a short-range bond-valence perspective, this structural model with a dominant A2 site provides a reasonable framework for the cation ordering involving the site configuration M4-O3-A of the present Pb^{2+}-bearing, Mn^{3+}-rich pargasite. Such a structural model is consistent with the Na content observed by EMP analysis, and demonstrate the occurrence of Pb^{2+} at the A site in the monoclinic *C*2/*m* amphibole structure. This is also in agreement with the ordering of Pb^{2+} at the A sites in the rare Pb^{2+}-bearing *P*2/*a* amphibole joesmithite (Moore et al. 1993), but it contrasts with an the suggested ordering of Pb^{2+} at the M4 site reported in some studies on element partitioning between amphiboles and melts (Brenan et al. 1995).

Bond-valence considerations and octahedral distortions

The bond-valence analysis for the studied Pb^{2+}-bearing, Mn^{3+}-rich pargasite was carried out using equations and bond-valence parameters from Brown and Altermatt (1985). The results (Table 6) are fully consistent with the proposed cation distributions. In particular, the bond-valence sums (BVS) incident at M1, M2, and M3 sites are significantly larger than 2 valence units, indicating the occurrence of trivalent cations at these octahedrally coordinated sites. BVS at O3 (1.06 valence units) is also consistent with the presence of OH, whereas the relative low BVS at O4 (1.88 valence units) is a characteristic of amphiboles (Hawthorne 1983) and relates to local strain in the structure rather than the presence of the other anions at O4.

Analysis of the distortions of the M1O₆, M2O₆, and M3O₆ polyhedra of the Pb^{2+}-bearing, Mn^{3+}-rich pargasite reveal a range of deviations from ideality (Table 4). The bond-length distortion, calculated by using the equation of Brown and Shannon (1973) show the order M3<M1<M2. In contrast, bond-angle distortion as well as the total octahedral distortion, calculated by the bond-angle variance and mean quadratic elongation formulas proposed by Robinson et al. (1971), show the order M2<M1<M3.

Nearest-neighbor (NN) and next-nearest-neighbor (NNN) configurations

The polarized single-crystal FTIR spectra collected in the OH stretching frequency range are comparable to the unpolarized spectra of pargasite dominant amphiboles along the join richterite-pargasite (Della Ventura et al. 1999). The strong polarization in **E‖α** of the observed OH stretching bands (Fig. 1) is a feature shared by most amphiboles and is explained by the strong alignment of the OH dipole nearly normal to the (100) (e.g., Skogby and Rossman 1991). The observed γ:α ratio for the integrated OH band absorption in the spectra of the present pargasite is 0.214, which compares very well with the corresponding value of 0.22 for richterite (Skogby and Rossman 1991). The OH stretching absorption in the third optical direction (β) is virtually zero.

The absorption bands in the obtained spectra can be fitted very well with Gaussian lineshapes using the positions for the OH stretching bands assigned to various nearest neighbor (NN) and next-nearest neighbor (NNN) configurations in richterite-pargasite join amphiboles as described by Della Ventura et al. (1999). In their assignment scheme, the band A is related to OH stretching associated with a MgMgMg-OH-^ANa:SiSi-MgMgMgMgMg [(M1M1M3)-OH-A:T1T1-[M2M2M3M2M2]] configuration that is a dominant feature in richterite, but cannot exist in pargasite end-member. From the fitted spectra (Fig. 2) and the retrieved band parameters (Table 7) it is evident that band A is indeed very weak (less than 4% of the total OH stretching absorbance). The band labeled E by Della Ventura et al. (1999) is related to OH stretching associated with a configuration involving exclusive Si occupancy of T1 and T2 sites in combination with vacant A sites. As the A site of the present pargasite is occupied by Na, Pb, and K and the T1 site has a high-Al occupancy (ca. 40%), and so we do not expect any significant E band contribution to the OH stretching spectrum. It is also noteworthy that the characteristic OH stretching band at ca. 3695 cm⁻¹ (Robert et al. 2000; Della Ventura et al. 2001) related to the inferred presence of F, and thereby OH-F anion arrangements, in pargasite is not observed in our spectra, which confirms the present EMP analyses demonstrating fluorine contents below the detection
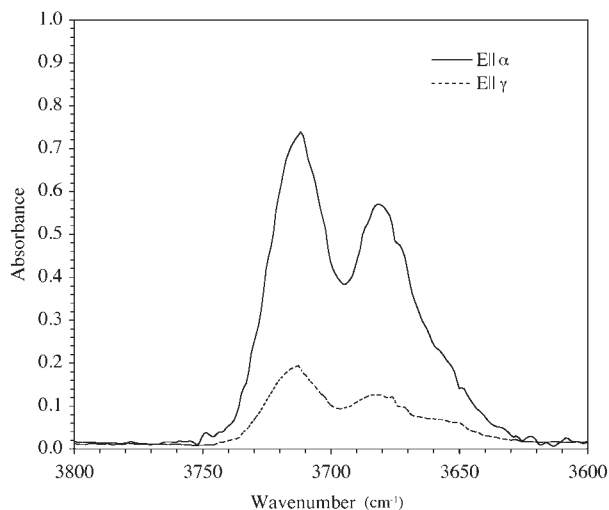
FIGURE 1. Polarized **E**∥α and **E**∥γ single-crystal FTIR spectra of the present pargasite in the OH stretching region.
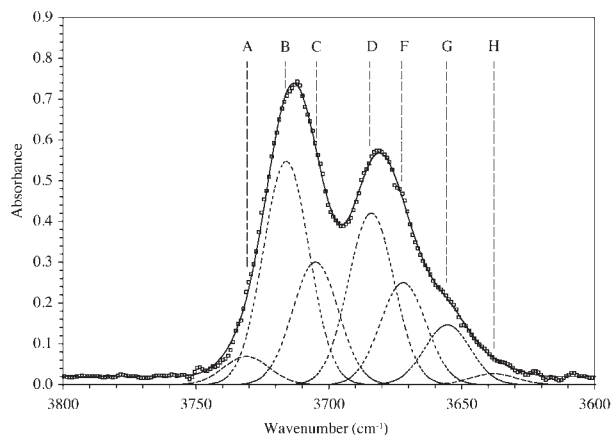

FIGURE 2. Band-resolved **E**∥α FTIR spectrum of the present pargasite in the OH stretching region. Squares represent experimental data, resolved component bands labeled A to H according to the assignment scheme of Della Ventura et al. (1999) are illustrated by broken lines and the resulting fitted spectrum is shown as a solid line.

limits of the method. The remaining fitted bands B, C, D, F, G, and H are all related to NNN configurations found in paragasite (Della Ventura et al. 1999).

For a qualitative analysis of the recorded OH stretching spectra, comparisons with the spectrum presented by Della Ventura et al. (1999) for their sample Pa(80) is the most appropriate as the present amphibole closely resembles this composition in terms of Al³⁺ for Si and M³⁺ for Mg substitutions. However, in our pargasite there is less Al³⁺ at M(1,2,3) sites [ca. 0.25 apfu compared to 0.8 apfu in Pa(80)] and Mn³⁺ and Fe³⁺ represent important replacements (ca. 0.5 pfu) for Mg at these sites. This difference in chemistry is expected to result in a modified OH stretching spectrum as compared to the Pa(80) sample of Della Ventura et al. (1999). The observed absorbance ratios for (D+F)/(B+C) of ca. 0.8 and (G+H)/(B+C) of ca. 0.2 differ indeed from those recorded by Della Ventura et al. (1999) in spectra of their

sample Pa(80). Their corresponding (D+F)/(B+C) band ratio for this composition equals 1.13 and bands G and H were only observed in the spectrum of their end-member pargasite but not in the spectrum of their sample Pa(80). Consequently, we can state that bands D and F, which are related to OH stretching associated with configurations involving Al at the M3 site (Della Ventura et al. 1999), are less intense in spectra of our pargasite relative to what is observed in pargasitic amphiboles where the M sites are only occupied by Mg and Al. We can also state that OH stretching bands at lower energies (bands G and H) are much more intense than those of spectra of pargasitic amphiboles lacking transition elements. The first of these two observations reflects a lower Al content of the present paragasite and hence a lower Al occupancy of M3 and does not contradict the previously reported Al disordering over M2 and M3 sites in Mg-rich pargasites (Oberti et al. 1995a). The observed strong enhancement of G and H band intensities may be explained by different cation ordering schemes. These two OH stretching bands may be related to NNN configurations [M2M2M3M2M2] involving trivalent cations (M³⁺) substituting for Mg at more than one M2 site (Della Ventura et al. 1999), e.g., M³⁺MgMgM³⁺Mg or M³⁺MgMgM³⁺M³⁺. Such assignments agree with our single-crystal X-ray diffraction and imply that the relative increase in intensity of G and H bands reflects ordering of M³⁺ cations at the M2 site. As the [6]Al content of our pargasite is low, it can be deduced that G and H band intensities are due to ordering of the additional [6]M³⁺ cations, Mn³⁺ and Fe³⁺, at the M2 site. However, interpretations of the FTIR spectra are complicated by the fact that OH stretching bands associated with nearest neighbor [M1M1M3] configurations involving trivalent transition metal cations, are shifted with respect to MgMgMg arrangements by ca. −50 cm⁻¹ (Raudsepp et al. 1987). Consequently, the observed relative increase in intensity of the G and H bands may also be caused by trivalent transition metal cations ordering at M1 and/or M3 sites. An additional possibility is that the G and H bands represent OH stretching modes related to MgMgMg arrangements coupled to vacant A sites. However, these two latter alternatives are considered less likely. The present structure refinement shows a high-A site occupancy in our pargasite, which rules out the vacancy alternative as an explanation for the intensified G and H bands. Furthermore, numerous studies of pargasite samples including crystal structure refinements (e.g., Welch et al. 1994; Tait et al. 2001) have demonstrated that Mg is strongly ordered at the M1 site. Our X-ray structure refinement of the present pargasite also shows a Mg site preference, M1>M2>M3, and an Mg occupancy of the M1 site of 0.9 in agreement with previous studies. In addition, our structure refinement demonstrate that the fractions of transition metals at M1 and M3 are low. Hence, NN configurations involving trivalent transition metal cations are expected to produce very limited contributions to the OH stretching spectra.

Local Mn³⁺-O bond lengths and distortion of the M2O₆ polyhedron

The mean M-O distance of the Mn³⁺-bearing M2O₆ polyhedron in our pargasite (2.075 Å) is clearly longer than those reported by Ghose et al. (1986) for Mn³⁺-bearing M2 sites in magnesio-riebeckite (2.051 Å) and magnesio-arfvedsonite

(2.041 Å). In addition, the bond length distortion (Brown and Shannon 1973) of the $M2O_6$ polyhedron in the present pargasite is calculated to be 0.000385. This value is considerably smaller than the bond-length distortion values of 0.00162–0.00194 calculated for the $M2O_6$ polyhedron in the amphiboles of Ghose et al. (1986). These findings contradict the suggestions made by Jonsson and Hålenius (2010) based upon optical absorption spectroscopy. The reason for this apparent contradiction is related to the contrasting probing sensitivity of the different methods. In the case of X-ray diffraction we record mean M-O distances for all $M2O_6$ polyhedra in the diffracting volume, while optical absorption spectra records electronic transitions in all Mn^{3+}-centered $M2O_6$ polyhedra, which in turn are related to the local Mn^{3+}-O distances and $Mn^{3+}O_6$-configurations. As the fraction of Mn^{3+}-centered M2 sites is less than 15% in our sample, it is clear that the mean M2-O bond distance determined by single-crystal X-ray refinement mainly represents the distances for the dominant Mg-centered M2 sites and is not representative of the local distances between Mn^{3+} at M2 and its surrounding oxygen atoms. If the amphibole structure were to follow Vegard's Rule, this technique-related difference would not be of importance. However, numerous studies have shown that structural relaxation (Urusov 1992) may be complete or nearly complete in solid solutions of oxygen-based mineral structures (e.g., Taran et al. 2004; Juhin et al. 2007; Hålenius et al. 2011) and consequently such differences become highly important. Complete structural relaxation may be vizualised as a hard-sphere case in which local bond-distances remain constant even along an entire solid-solution series. As the fraction of trivalent transition metal cations at M2 sites is much higher (53–69%) in the amphiboles of Ghose et al. (1986), the comparison between mean M2-O distances and octahedral distortion in the present pargasite and in those amphiboles is not relevant for obtaining a comparative view of the local Mn^{3+}-O configuration at the M2 site. Consequently, the apparent contradiction between results obtained by optical absorption spectroscopy and X-ray diffraction methods indicates that the structural relaxation of the $M2-O_6$ polyhedron in $C2/m$ amphiboles is very strong, perhaps even complete or nearly so.

REFERENCES CITED

Armstrong, J.T. (1995) CITZAF: a package of correction programs for the quantitative electron microbeam X-ray-analysis of thick polished materials, thin films, and particles. Microbeam Analysis, 4, 177–200.
Brenan, J.M., Shaw, H.F., Ryerson, F.J., and Phinney, D.L. (1995) Experimental determination of trace-element partitioning between pargasite and a synthetic hydrous andesitic melt. Earth and Planetary Science Letter, 135, 1–11.
Brown, I.D. and Altermatt, D. (1985) Bond-valence parameters obtained from a systematic analysis of the Inorganic Crystal Structure Database. Acta Crystallographica B, 41, 244–247.
Brown, I.D. and Shannon, R.D. (1973) Empirical bond-strength bond-length curves for oxides. Acta Crystallographica, A29, 266–282.
Della Ventura, G., Hawthorne, F.C., Robert, J.-L., Delbove, F., Welch, M.D., and Raudsepp, M. (1999) Short-range order of cations in synthetic amphiboles along the richterite-pargasite join. European Journal of Mineralogy, 11, 79–94.
Della Ventura, G., Robert, J.-L., Sergent, J., Hawthorne, F.C., and Delbove, F. (2001) Constraints on F vs. OH incorporation in synthetic [6]Al-bearing in monoclinic amphiboles. European Journal of Mineralogy, 13, 841–847.
Ghose, S., Kersten, M., Langer, K., Rossi, G., and Ungaretti, L. (1986) Crystal field spectra and Jahn Teller effect of Mn^{3+} in clinopyroxene and clinoamphiboles from India. Physics and Chemistry of Minerals, 13, 291–305.
Hålenius, U., Bosi, F., and Skogby, H. (2011) A first record of strong structural relaxation of TO_4 tetrahedra in a spinel solid solution. American Mineralogist, 96, 617–622.
Hawthorne, F.C. (1983) Crystal chemistry of the amphiboles. Canadian Mineralogist, 21, 173–480.
Hawthorne, F.C. and Harlow, G.E. (2008) The crystal chemistry of Al-rich amphiboles: sadanagaite and potassic-ferrisadanagaite. Canadian Mineralogist, 46, 151–162.
Hawthorne, F.C., Oberti, R., Cannillo, E., Sardone, N., Zanetti, A., Grice, J.D., and Ashley, P.M. (1995) A new anhydrous amphibole from the Hoskins mine, Grenfell, New South Wales, Australia: Description and crystal structure of ungarettiite, $NaNa_2(Mn_2^{2+}Mn_3^{3+})Si_8O_{22}O_2$. American Mineralogist, 80, 165–172.
Hawthorne, F.C., Oberti, R., and Sardone, N. (1996) Sodium at the A site in clinoamphiboles: the effects of composition on patterns of order. Canadian Mineralogist, 34, 577–593.
Hawthorne, F.C., Cooper, M.A., Grice, J.D., and Ottolini, L. (2000) A new anhydrous amphibole from the Eifel region, Germany: description and crystal structure of obertiite, $NaNa_2(Mg_3Fe^{3+}Ti^{4+})Si_8O_{22}O_2$. American Mineralogist, 85, 236–241.
Jonsson, E. and Hålenius, U. (2010) Mn^{3+}-bearing pargasite from the Långban Fe-Mn oxide mineralisation, Bergslagen, Sweden. GFF, 132, 167–172.
Juhin, A., Calas, G., Cabaret, D., Galoisy, L., and Hazemann, J.-L. (2007) Structural relaxation around substitutional Cr^{3+} in $MgAl_2O_4$. Physical Review B, 76, 054105.
Moore, P.B., Davis, A.M., Van Derveer, D.G., and Sen Gupta, P.K. (1993) Joesmithite, a plumbous amphibole revisited and comments on bond valences. Mineralogy and Petrology, 48, 97–113.
Oberti, R. and Ghose, S. (1993) Crystal chemistry of a complex Mn-bearing alkali amphibole ("tirodite") on the verge of exsolution. European Journal of Mineralogy, 5, 1153–1160.
Oberti, R., Hawthorne, F.C., Ungaretti, L., and Canillo, E. (1993) The behaviour of Mn in amphiboles: Mn in richterite. European Journal of Mineralogy, 5, 43–51.
Oberti, R., Hawthorne, F.C., Ungaretti, L., and Cannillo, E. (1995a) [6]Al disorder in amphiboles from mantle peridotites. Canadian Mineralogist, 33, 867–878.
Oberti, R., Sardone, N., Hawthorne, F.C., Raudsepp, M., and Turnock, A.C. (1995b) Synthesis and crystal-structure refinement of synthetic fluor-pargasite. Canadian Mineralogist, 33, 25–31.
Oberti, R., Cámara, F., Della Ventura, G., Iezzi, G., and Benimoff, A.I. (2006) Parvo-mangano-edenite, parvo-manganotremolite, and the solid solution between Ca and Mn^{2+} at the M4 site in amphiboles. American Mineralogist, 91, 526–532.
Oberti, R., Hawthorne, F.C., Canillo, E., and Càmara, F. (2007) Long-range order in amphiboles. In F.C. Hawthorne, R. Oberti, G. Della Ventura, A. Mottana, Eds., Amphiboles: Crystal Chemistry, Occurrence, and Health Issues, 67, p. 125–171. Reviews in Mineralogy, Mineralogical Society of America, Chantilly, Virginia.
Raudsepp, M., Turnock, A.C., Hawthorne, F.C., Sherriff, B.L., and Hartman, J.S. (1987) Characterization of synthetic pargasitic amphiboles $NaCa_2Mg_4M^{3+}Si_6Al_2O_{22}$ $(OH,F)_2$; M^{3+} = Al, Cr, Ga, Sc, In) by infrared spectroscopy, Rietveld structure refinement, and ^{27}Al, ^{29}Si, and ^{19}F MAS NMR spectroscopy. American Mineralogist, 72, 580–593.
Robert, J.-L., Della Ventura, G., Welch, M.D., and Hawthorne, F.C. (2000) The OH–F substitution in synthetic pargasite at 1.5 kbar, 850°C. American Mineralogist, 85, 926–931.
Robinson, K., Gibbs, G.V., and Ribbe, P.H. (1971) Quadratic elongation: A quantitative measure of distortion in coordination polyhedra. Science, 172, 567–570.
Shannon, R.D. (1976) Revised effective ionic radii and systematic studies of interatomic distances in halides and chalcogenides. Acta Crystallographica, A32, 751–767.
Sheldrick, G.M. (2008) A short history of SHELX. Acta Crystallographica, A64, 112–122.
Skogby, H. and Rossman, G.R. (1991) The intensity of amphibole OH bands in the infrared absorption spectrum. Physics and Chemistry of Minerals, 18, 64–68.
Tait, K.T., Hawthorne, F.C., and Della Ventura, G. (2001) Al-Mg disorder in gem-quality pargasite from Baffin Island, Nunavut, Canada. Canadian Mineralogist, 39, 1725–1732.
Tait, K.T., Hawthorne, F.C., Grice, J.D., Ottolini, L., and Nayak, V.K. (2005) Dellaventuraite, $NaNa_2(MgMn_3^{3+}Ti^{4+}Li)Si_8O_{22}O_2$, a new anhydrous amphibole from the Kajlidongri Manganese Mine, Jhabua District, Madhya Pradesh, India. American Mineralogist, 90, 304–309.
Taran, M.N., Langer, K., Abs-Wurmbach, I., Frost, D.J., and Platonov, A.N. (2004) Local relaxation around [6]Cr^{3+} in synthetic pyrope-knorringite garnets, [8]Mg_3 [6]$(Al_{1-X}Cr_X^{3+})_2$[4]Si_3O_{12}, from electronic absorption spectra. Physics and Chemistry of Minerals, 31, 650–657.
Urusov, V.S. (1992) A geometric model of deviations from Vegard's rule. Journal of Solid State Chemistry, 98, 223–236.
Welch, M.D., Kolodziejski, W., and Klinowski, J. (1994) A multinuclear NMR study of synthetic pargasite. American Mineralogist, 79, 261–268.

data_mn_pargasite

_audit_creation_method   SHELXL-97
_chemical_name_systematic
;
 ?
;
_chemical_name_common   ?
_chemical_melting_point   ?
_chemical_formula_moiety   ?
_chemical_formula_sum
 'H2 Ca2 Mg5 Mn0.50 Na3 O224 Si6'
_chemical_formula_weight   852.68

loop_
 _atom_type_symbol
 _atom_type_description
 _atom_type_scat_dispersion_real
 _atom_type_scat_dispersion_imag
 _atom_type_scat_source
 'O' 'O2'   0.0080   0.0060
 'International Tables Vol C Tables 4.2.6.8 and 6.1.1.4'
 'H' 'H'   0.0000   0.0000
 'International Tables Vol C Tables 4.2.6.8 and 6.1.1.4'
 'Na' 'Na'   0.0362   0.0249
 'International Tables Vol C Tables 4.2.6.8 and 6.1.1.4'
 'Mg' 'Mg'   0.0486   0.0363
 'International Tables Vol C Tables 4.2.6.8 and 6.1.1.4'
 'Si' 'Si'   0.0817   0.0704
 'International Tables Vol C Tables 4.2.6.8 and 6.1.1.4'
 'Ca' 'Ca'   0.2262   0.3064
 'International Tables Vol C Tables 4.2.6.8 and 6.1.1.4'
 'Mn' 'Mn'   0.3368   0.7283
 'International Tables Vol C Tables 4.2.6.8 and 6.1.1.4'

_symmetry_cell_setting   ?
_symmetry_space_group_name_H-M   ?

loop_
 _symmetry_equiv_pos_as_xyz
 'x, y, z'
 '-x, y, -z'
 'x+1/2, y+1/2, z'
 '-x+1/2, y+1/2, -z'
 '-x, -y, -z'
 'x, -y, z'
 '-x+1/2, -y+1/2, -z'
 'x+1/2, -y+1/2, z'

_cell_length_a   9.9448(5)
_cell_length_b   18.0171(9)
_cell_length_c   5.2829(3)
_cell_angle_alpha   90.00
_cell_angle_beta   105.445(2)
_cell_angle_gamma   90.00

```
_cell_volume                       912.39(8)
_cell_formula_units_Z              2
_cell_measurement_temperature      293(2)
_cell_measurement_reflns_used      ?
_cell_measurement_theta_min        ?
_cell_measurement_theta_max        ?

_exptl_crystal_description         ?
_exptl_crystal_colour              ?
_exptl_crystal_size_max            0.12
_exptl_crystal_size_mid            0.10
_exptl_crystal_size_min            0.05
_exptl_crystal_density_meas        ?
_exptl_crystal_density_diffrn      3.104
_exptl_crystal_density_method      'not measured'
_exptl_crystal_F_000               943
_exptl_absorpt_coefficient_mu      2.035
_exptl_absorpt_correction_type     ?
_exptl_absorpt_correction_T_min    0.7923
_exptl_absorpt_correction_T_max    0.9051
_exptl_absorpt_process_details     ?

_exptl_special_details
;
 ?
;

_diffrn_ambient_temperature        293(2)
_diffrn_radiation_wavelength       0.71073
_diffrn_radiation_type             MoK\a
_diffrn_radiation_source           'fine-focus sealed tube'
_diffrn_radiation_monochromator    graphite
_diffrn_measurement_device_type    ?
_diffrn_measurement_method         ?
_diffrn_detector_area_resol_mean   ?
_diffrn_standards_number           ?
_diffrn_standards_interval_count   ?
_diffrn_standards_interval_time    ?
_diffrn_standards_decay_%          ?
_diffrn_reflns_number              23890
_diffrn_reflns_av_R_equivalents    0.0172
_diffrn_reflns_av_sigmaI/netI      0.0109
_diffrn_reflns_limit_h_min         -16
_diffrn_reflns_limit_h_max         14
_diffrn_reflns_limit_k_min         -32
_diffrn_reflns_limit_k_max         31
_diffrn_reflns_limit_l_min         -9
_diffrn_reflns_limit_l_max         9
_diffrn_reflns_theta_min           2.26
_diffrn_reflns_theta_max           39.39
_reflns_number_total               2675
_reflns_number_gt                  2429
_reflns_threshold_expression       >2sigma(I)

_computing_data_collection         ?
_computing_cell_refinement         ?
_computing_data_reduction          ?
```

```
_computing_structure_solution      'SHELXS-97 (Sheldrick, 1990)'
_computing_structure_refinement    'SHELXL-97 (Sheldrick, 1997)'
_computing_molecular_graphics      ?
_computing_publication_material    ?

_refine_special_details
;
 Refinement of F^2^ against ALL reflections.  The weighted R-factor wR and
 goodness of fit S are based on F^2^, conventional R-factors R are based
 on F, with F set to zero for negative F^2^. The threshold expression of
 F^2^ > 2sigma(F^2^) is used only for calculating R-factors(gt) etc. and is
 not relevant to the choice of reflections for refinement.  R-factors based
 on F^2^ are statistically about twice as large as those based on F, and R-
 factors based on ALL data will be even larger.
;

_refine_ls_structure_factor_coef   Fsqd
_refine_ls_matrix_type             full
_refine_ls_weighting_scheme        calc
_refine_ls_weighting_details
 'calc w=1/[\s^2^(Fo^2^)+(0.0250P)^2^+1.4869P] where P=(Fo^2^+2Fc^2^)/3'
_atom_sites_solution_primary       direct
_atom_sites_solution_secondary     difmap
_atom_sites_solution_hydrogens     geom
_refine_ls_hydrogen_treatment      mixed
_refine_ls_extinction_method       SHELXL
_refine_ls_extinction_coef         0.0029(3)
_refine_ls_extinction_expression
 'Fc^*^=kFc[1+0.001xFc^2^\l^3^/sin(2\q)]^-1/4^'
_refine_ls_number_reflns           2675
_refine_ls_number_parameters       111
_refine_ls_number_restraints       1
_refine_ls_R_factor_all            0.0264
_refine_ls_R_factor_gt             0.0233
_refine_ls_wR_factor_ref           0.0599
_refine_ls_wR_factor_gt            0.0586
_refine_ls_goodness_of_fit_ref     1.058
_refine_ls_restrained_S_all        1.057
_refine_ls_shift/su_max            0.001
_refine_ls_shift/su_mean           0.000

loop_
 _atom_site_label
 _atom_site_type_symbol
 _atom_site_fract_x
 _atom_site_fract_y
 _atom_site_fract_z
 _atom_site_U_iso_or_equiv
 _atom_site_adp_type
 _atom_site_occupancy
 _atom_site_symmetry_multiplicity
 _atom_site_calc_flag
 _atom_site_refinement_flags
 _atom_site_disorder_assembly
 _atom_site_disorder_group
A2 Na 0.0000 0.47416(10) 0.0000 0.0639(8) Uani 0.723(5) 2 d SP . .
M1 Mg 0.0000 0.08888(2) 0.5000 0.00625(11) Uani 1.078(3) 2 d SP . .
```

```
M2 Mg 0.0000 0.17595(2) 0.0000 0.00512(10) Uani 1.147(3) 2 d SP . .
M3 Mg 0.0000 0.0000 0.0000 0.00577(15) Uani 1.059(4) 4 d SP . .
M4 Ca 0.0000 0.27952(3) 0.5000 0.00906(7) Uani 0.9660(19) 2 d SP . .
M4' Mn 0.0000 0.2628(8) 0.5000 0.011(2) Uiso 0.0340(19) 2 d SP . .
T1 Si 0.27974(3) 0.084887(14) 0.30315(5) 0.00699(7) Uani 0.9694(18) 1 d P . .
T2 Si 0.28968(3) 0.172538(13) 0.81127(5) 0.00629(6) Uani 1 1 d . . .
O1 O2 0.10767(7) 0.08634(4) 0.21947(13) 0.00906(11) Uani 1 1 d . . .
O2 O2 0.12024(7) 0.17250(4) 0.72790(12) 0.00764(10) Uani 1 1 d . . .
O3 O2 0.10770(10) 0.0000 0.71802(19) 0.00891(15) Uani 1 2 d S . .
H3 H 0.210(3) 0.0000 0.766(5) 0.013 Uiso 1 2 d S . .
O4 O2 0.36588(8) 0.24907(4) 0.78694(13) 0.01007(11) Uani 1 1 d . . .
O5 O2 0.34870(7) 0.13969(4) 0.11256(13) 0.01141(12) Uani 1 1 d . . .
O6 O2 0.34450(8) 0.11446(4) 0.61330(14) 0.01185(12) Uani 1 1 d . . .
O7 O2 0.34069(11) 0.0000 0.2734(2) 0.01322(17) Uani 1 2 d S . .

loop_
 _atom_site_aniso_label
 _atom_site_aniso_U_11
 _atom_site_aniso_U_22
 _atom_site_aniso_U_33
 _atom_site_aniso_U_23
 _atom_site_aniso_U_13
 _atom_site_aniso_U_12
A2 0.0289(8) 0.0484(10) 0.124(2) 0.000 0.0377(10) 0.000
M1 0.00750(19) 0.00632(17) 0.00527(16) 0.000 0.00227(13) 0.000
M2 0.00560(18) 0.00512(15) 0.00486(15) 0.000 0.00175(11) 0.000
M3 0.0067(3) 0.0056(2) 0.0050(2) 0.000 0.00165(18) 0.000
M4 0.01127(13) 0.00743(15) 0.01008(11) 0.000 0.00564(8) 0.000
T1 0.00661(12) 0.00708(10) 0.00712(10) −0.00030(7) 0.00154(8) −0.00048(7)
T2 0.00609(11) 0.00688(9) 0.00595(9) 0.00010(6) 0.00168(7) −0.00047(7)
O1 0.0078(3) 0.0108(2) 0.0084(2) 0.00018(18) 0.0017(2) −0.0010(2)
O2 0.0057(3) 0.0091(2) 0.0079(2) 0.00034(18) 0.00138(19) 0.00018(18)
O3 0.0069(4) 0.0095(3) 0.0102(3) 0.000 0.0019(3) 0.000
O4 0.0115(3) 0.0085(2) 0.0109(2) −0.00036(19) 0.0041(2) −0.0026(2)
O5 0.0093(3) 0.0150(3) 0.0089(2) 0.0048(2) 0.0004(2) −0.0004(2)
O6 0.0088(3) 0.0139(3) 0.0129(3) −0.0051(2) 0.0029(2) 0.0008(2)
O7 0.0094(4) 0.0129(4) 0.0169(4) 0.000 0.0029(3) 0.000

_geom_special_details
;
 All esds (except the esd in the dihedral angle between two l.s. planes)
 are estimated using the full covariance matrix.  The cell esds are taken
 into account individually in the estimation of esds in distances, angles
 and torsion angles; correlations between esds in cell parameters are only
 used when they are defined by crystal symmetry.  An approximate (isotropic)
 treatment of cell esds is used for estimating esds involving l.s. planes.
;

loop_
 _geom_bond_atom_site_label_1
 _geom_bond_atom_site_label_2
 _geom_bond_distance
 _geom_bond_site_symmetry_2
 _geom_bond_publ_flag
A2 A2 0.931(4) 5_565 ?
A2 O7 2.4558(11) 7 ?
A2 O7 2.4558(11) 3_455 ?
```

```
A2 O5 2.7022(16) 8_455 ?
A2 O5 2.7022(16) 7 ?
A2 O6 2.7261(13) 8_454 ?
A2 O6 2.7261(13) 7_556 ?
A2 T1 3.2192(7) 8_455 ?
A2 T1 3.2192(7) 7 ?
A2 T2 3.3533(14) 8_454 ?
A2 T2 3.3533(14) 7_556 ?
M1 O1 2.0469(7) . ?
M1 O1 2.0469(7) 2_556 ?
M1 O3 2.0932(7) . ?
M1 O3 2.0932(7) 5_556 ?
M1 O2 2.0933(7) . ?
M1 O2 2.0934(7) 2_556 ?
M1 M2 3.0721(3) 1_556 ?
M1 M2 3.0721(3) . ?
M1 M3 3.0890(2) . ?
M1 M3 3.0890(2) 1_556 ?
M1 M1 3.2028(8) 5_556 ?
M2 O4 2.0176(7) 7_556 ?
M2 O4 2.0176(7) 8_454 ?
M2 O2 2.1013(7) 2_556 ?
M2 O2 2.1013(7) 1_554 ?
M2 O1 2.1062(7) . ?
M2 O1 2.1062(7) 2 ?
M2 M1 3.0721(3) 1_554 ?
M2 M3 3.1701(4) . ?
M2 M4 3.2341(4) . ?
M3 O3 2.0534(10) 5_556 ?
M3 O3 2.0534(10) 1_554 ?
M3 O1 2.0614(7) 5 ?
M3 O1 2.0614(7) 6 ?
M3 O1 2.0614(7) 2 ?
M3 O1 2.0615(7) . ?
M3 M1 3.0890(2) 5 ?
M3 M1 3.0890(2) 5_556 ?
M3 M1 3.0890(2) 1_554 ?
M3 M2 3.1701(4) 5 ?
M4 O4 2.3279(7) 8_455 ?
M4 O4 2.3279(7) 7_556 ?
M4 O2 2.4147(8) 2_556 ?
M4 O2 2.4147(8) . ?
M4 O6 2.6250(8) 7_556 ?
M4 O6 2.6250(8) 8_455 ?
M4 O5 2.6329(8) 7_556 ?
M4 O5 2.6329(8) 8_455 ?
M4 T2 3.1076(3) 7_556 ?
M4 T2 3.1076(3) 8_455 ?
M4 M2 3.2341(4) 1_556 ?
M4' O2 2.1823(108) 2_556 ?
M4' O2 2.1823(108) . ?
M4' O4 2.2803(15) 8_455 ?
M4' O4 2.2803(15) 7_556 ?
T1 O1 1.6497(7) . ?
T1 O7 1.6679(5) . ?
T1 O6 1.6797(7) . ?
T1 O5 1.6812(7) . ?
```

```
T1 A2 3.2192(7) 7 ?
T1 M4 3.2610(5) 7_556 ?
T2 O4 1.5950(7) . ?
T2 O2 1.6242(7) . ?
T2 O5 1.6525(7) 1_556 ?
T2 O6 1.6702(7) . ?
T2 M4 3.1075(3) 7_556 ?
T2 A2 3.3533(14) 7_556 ?
O2 M2 2.1013(7) 1_556 ?
O3 M3 2.0533(10) 1_556 ?
O3 M1 2.0931(7) 5_556 ?
O3 H3 0.98(2) . ?
O4 M2 2.0177(7) 7_556 ?
O4 M4 2.3279(7) 7_556 ?
O5 T2 1.6525(7) 1_554 ?
O5 M4 2.6328(8) 7_556 ?
O5 A2 2.7022(16) 7 ?
O6 M4 2.6250(8) 7_556 ?
O6 A2 2.7262(13) 7_556 ?
O7 T1 1.6679(5) 6 ?
O7 A2 2.4559(11) 3_545 ?
O7 A2 2.4559(11) 7 ?


loop_
 _geom_angle_atom_site_label_1
 _geom_angle_atom_site_label_2
 _geom_angle_atom_site_label_3
 _geom_angle
 _geom_angle_site_symmetry_1
 _geom_angle_site_symmetry_3
 _geom_angle_publ_flag
A2 A2 O7 79.07(4) 5_565 7 ?
A2 A2 O7 79.07(4) 5_565 3_455 ?
O7 A2 O7 158.15(8) 7 3_455 ?
A2 A2 O5 139.38(3) 5_565 8_455 ?
O7 A2 O5 139.25(6) 7 8_455 ?
O7 A2 O5 61.98(2) 3_455 8_455 ?
A2 A2 O5 139.38(3) 5_565 7 ?
O7 A2 O5 61.98(2) 7 7 ?
O7 A2 O5 139.25(6) 3_455 7 ?
O5 A2 O5 81.23(6) 8_455 7 ?
A2 A2 O6 125.86(3) 5_565 8_454 ?
O7 A2 O6 89.79(3) 7 8_454 ?
O7 A2 O6 103.04(3) 3_455 8_454 ?
O5 A2 O6 58.82(3) 8_455 8_454 ?
O5 A2 O6 68.19(4) 7 8_454 ?
A2 A2 O6 125.86(3) 5_565 7_556 ?
O7 A2 O6 103.04(3) 7 7_556 ?
O7 A2 O6 89.79(3) 3_455 7_556 ?
O5 A2 O6 68.19(4) 8_455 7_556 ?
O5 A2 O6 58.82(3) 7 7_556 ?
O6 A2 O6 108.29(7) 8_454 7_556 ?
A2 A2 T1 109.30(3) 5_565 8_455 ?
O7 A2 T1 170.47(6) 7 8_455 ?
O7 A2 T1 30.581(13) 3_455 8_455 ?
O5 A2 T1 31.473(16) 8_455 8_455 ?
O5 A2 T1 110.56(6) 7 8_455 ?
```

```
O6 A2 T1 81.60(3) 8_454 8_455 ?
O6 A2 T1 76.05(3) 7_556 8_455 ?
A2 A2 T1 109.30(3) 5_565 7 ?
O7 A2 T1 30.581(13) 7 7 ?
O7 A2 T1 170.47(6) 3_455 7 ?
O5 A2 T1 110.56(6) 8_455 7 ?
O5 A2 T1 31.473(16) 7 7 ?
O6 A2 T1 76.05(3) 8_454 7 ?
O6 A2 T1 81.60(3) 7_556 7 ?
T1 A2 T1 141.40(6) 8_455 7 ?
A2 A2 T2 142.020(19) 5_565 8_454 ?
O7 A2 T2 115.06(4) 7 8_454 ?
O7 A2 T2 82.84(3) 3_455 8_454 ?
O5 A2 T2 29.22(2) 8_455 8_454 ?
O5 A2 T2 71.10(4) 7 8_454 ?
O6 A2 T2 29.66(2) 8_454 8_454 ?
O6 A2 T2 86.88(5) 7_556 8_454 ?
T1 A2 T2 55.54(2) 8_455 8_454 ?
T1 A2 T2 92.57(4) 7 8_454 ?
A2 A2 T2 142.02(2) 5_565 7_556 ?
O7 A2 T2 82.84(3) 7 7_556 ?
O7 A2 T2 115.06(4) 3_455 7_556 ?
O5 A2 T2 71.10(4) 8_455 7_556 ?
O5 A2 T2 29.22(2) 7 7_556 ?
O6 A2 T2 86.88(5) 8_454 7_556 ?
O6 A2 T2 29.66(2) 7_556 7_556 ?
T1 A2 T2 92.57(4) 8_455 7_556 ?
T1 A2 T2 55.54(2) 7 7_556 ?
T2 A2 T2 75.96(4) 8_454 7_556 ?
O1 M1 O1 177.44(4) . 2_556 ?
O1 M1 O3 95.26(3) . . ?
O1 M1 O3 82.77(3) 2_556 . ?
O1 M1 O3 82.77(3) . 5_556 ?
O1 M1 O3 95.25(3) 2_556 5_556 ?
O3 M1 O3 80.17(4) . 5_556 ?
O1 M1 O2 95.95(3) . . ?
O1 M1 O2 85.90(3) 2_556 . ?
O3 M1 O2 95.96(3) . . ?
O3 M1 O2 175.77(3) 5_556 . ?
O1 M1 O2 85.90(3) . 2_556 ?
O1 M1 O2 95.95(3) 2_556 2_556 ?
O3 M1 O2 175.78(3) . 2_556 ?
O3 M1 O2 95.96(3) 5_556 2_556 ?
O2 M1 O2 87.95(4) . 2_556 ?
O1 M1 M2 138.91(2) . 1_556 ?
O1 M1 M2 43.04(2) 2_556 1_556 ?
O3 M1 M2 91.99(2) . 1_556 ?
O3 M1 M2 138.30(3) 5_556 1_556 ?
O2 M1 M2 43.013(19) . 1_556 ?
O2 M1 M2 89.79(2) 2_556 1_556 ?
O1 M1 M2 43.04(2) . . ?
O1 M1 M2 138.91(2) 2_556 . ?
O3 M1 M2 138.30(3) . . ?
O3 M1 M2 91.99(2) 5_556 . ?
O2 M1 M2 89.79(2) . . ?
O2 M1 M2 43.014(19) 2_556 . ?
M2 M1 M2 118.591(18) 1_556 . ?
```

```
O1 M1 M3 41.425(19) . . ?
O1 M1 M3 136.60(2) 2_556 . ?
O3 M1 M3 87.56(3) . . ?
O3 M1 M3 41.35(3) 5_556 . ?
O2 M1 M3 137.293(18) . . ?
O2 M1 M3 90.651(18) 2_556 . ?
M2 M1 M3 179.477(14) 1_556 . ?
M2 M1 M3 61.932(7) . . ?
O1 M1 M3 136.60(2) . 1_556 ?
O1 M1 M3 41.425(19) 2_556 1_556 ?
O3 M1 M3 41.35(3) . 1_556 ?
O3 M1 M3 87.56(3) 5_556 1_556 ?
O2 M1 M3 90.650(18) . 1_556 ?
O2 M1 M3 137.293(18) 2_556 1_556 ?
M2 M1 M3 61.932(7) 1_556 1_556 ?
M2 M1 M3 179.478(14) . 1_556 ?
M3 M1 M3 117.546(13) . 1_556 ?
O1 M1 M1 88.72(2) . 5_556 ?
O1 M1 M1 88.72(2) 2_556 5_556 ?
O3 M1 M1 40.09(2) . 5_556 ?
O3 M1 M1 40.09(2) 5_556 5_556 ?
O2 M1 M1 136.025(19) . 5_556 ?
O2 M1 M1 136.027(19) 2_556 5_556 ?
M2 M1 M1 120.705(9) 1_556 5_556 ?
M2 M1 M1 120.705(9) . 5_556 ?
M3 M1 M1 58.773(7) . 5_556 ?
M3 M1 M1 58.773(7) 1_556 5_556 ?
M4' M1 M1 180.0 . 5_556 ?
O4 M2 O4 95.94(4) 7_556 8_454 ?
O4 M2 O2 92.88(3) 7_556 2_556 ?
O4 M2 O2 89.39(3) 8_454 2_556 ?
O4 M2 O2 89.39(3) 7_556 1_554 ?
O4 M2 O2 92.88(3) 8_454 1_554 ?
O2 M2 O2 176.61(4) 2_556 1_554 ?
O4 M2 O1 92.43(3) 7_556 . ?
O4 M2 O1 169.71(3) 8_454 . ?
O2 M2 O1 84.22(3) 2_556 . ?
O2 M2 O1 93.18(3) 1_554 . ?
O4 M2 O1 169.71(3) 7_556 2 ?
O4 M2 O1 92.43(3) 8_454 2 ?
O2 M2 O1 93.18(3) 2_556 2 ?
O2 M2 O1 84.22(3) 1_554 2 ?
O1 M2 O1 79.91(4) . 2 ?
O4 M2 M1 90.78(2) 7_556 . ?
O4 M2 M1 132.08(2) 8_454 . ?
O2 M2 M1 42.813(19) 2_556 . ?
O2 M2 M1 134.70(2) 1_554 . ?
O1 M2 M1 41.554(19) . . ?
O1 M2 M1 88.02(2) 2 . ?
O4 M2 M1 132.08(2) 7_556 1_554 ?
O4 M2 M1 90.78(2) 8_454 1_554 ?
O2 M2 M1 134.70(2) 2_556 1_554 ?
O2 M2 M1 42.813(19) 1_554 1_554 ?
O1 M2 M1 88.02(2) . 1_554 ?
O1 M2 M1 41.554(19) 2 1_554 ?
M1 M2 M1 118.590(18) . 1_554 ?
O4 M2 M3 132.03(2) 7_556 . ?
```

```
O4 M2 M3 132.03(2) 8_454 . ?
O2 M2 M3 88.31(2) 2_556 . ?
O2 M2 M3 88.31(2) 1_554 . ?
O1 M2 M3 39.956(19) . . ?
O1 M2 M3 39.956(19) 2 . ?
M1 M2 M3 59.295(9) . . ?
M1 M2 M3 59.295(9) 1_554 . ?
O4 M2 M4 45.72(2) 7_556 . ?
O4 M2 M4 85.73(2) 8_454 . ?
O2 M2 M4 48.285(19) 2_556 . ?
O2 M2 M4 134.39(2) 1_554 . ?
O1 M2 M4 95.926(19) . . ?
O1 M2 M4 141.383(19) 2 . ?
M1 M2 M4 65.945(10) . . ?
M1 M2 M4 175.466(15) 1_554 . ?
M3 M2 M4 125.240(9) . . ?
O3 M3 O3 180.00(4) 5_556 1_554 ?
O3 M3 O1 96.60(3) 5_556 5 ?
O3 M3 O1 83.40(3) 1_554 5 ?
O3 M3 O1 83.40(3) 5_556 6 ?
O3 M3 O1 96.60(3) 1_554 6 ?
O1 M3 O1 82.01(4) 5 6 ?
O3 M3 O1 96.60(3) 5_556 2 ?
O3 M3 O1 83.40(3) 1_554 2 ?
O1 M3 O1 97.99(4) 5 2 ?
O1 M3 O1 180.00(4) 6 2 ?
O3 M3 O1 83.40(3) 5_556 . ?
O3 M3 O1 96.60(3) 1_554 . ?
O1 M3 O1 180.00(3) 5 . ?
O1 M3 O1 97.99(4) 6 . ?
O1 M3 O1 82.01(4) 2 . ?
O3 M3 M1 137.661(18) 5_556 5 ?
O3 M3 M1 42.339(18) 1_554 5 ?
O1 M3 M1 41.070(19) 5 5 ?
O1 M3 M1 88.365(19) 6 5 ?
O1 M3 M1 91.635(19) 2 5 ?
O1 M3 M1 138.930(19) . 5 ?
O3 M3 M1 42.339(18) 5_556 5_556 ?
O3 M3 M1 137.661(18) 1_554 5_556 ?
O1 M3 M1 88.365(19) 5 5_556 ?
O1 M3 M1 41.070(19) 6 5_556 ?
O1 M3 M1 138.930(19) 2 5_556 ?
O1 M3 M1 91.636(19) . 5_556 ?
M1 M3 M1 117.547(13) 5 5_556 ?
O3 M3 M1 137.661(18) 5_556 1_554 ?
O3 M3 M1 42.339(18) 1_554 1_554 ?
O1 M3 M1 91.635(19) 5 1_554 ?
O1 M3 M1 138.930(19) 6 1_554 ?
O1 M3 M1 41.070(19) 2 1_554 ?
O1 M3 M1 88.364(19) . 1_554 ?
M1 M3 M1 62.453(13) 5 1_554 ?
M1 M3 M1 180.000(13) 5_556 1_554 ?
O3 M3 M1 42.339(18) 5_556 . ?
O3 M3 M1 137.661(18) 1_554 . ?
O1 M3 M1 138.930(19) 5 . ?
O1 M3 M1 91.636(19) 6 . ?
O1 M3 M1 88.364(19) 2 . ?
```

```
O1 M3 M1 41.070(19) . . ?
M1 M3 M1 180.0 5 . ?
M1 M3 M1 62.454(13) 5_556 . ?
M1 M3 M1 117.546(13) 1_554 . ?
O3 M3 M2 90.0 5_556 5 ?
O3 M3 M2 90.0 1_554 5 ?
O1 M3 M2 41.007(19) 5 5 ?
O1 M3 M2 41.007(19) 6 5 ?
O1 M3 M2 138.993(19) 2 5 ?
O1 M3 M2 138.994(19) . 5 ?
M1 M3 M2 58.773(6) 5 5 ?
M1 M3 M2 58.773(7) 5_556 5 ?
M1 M3 M2 121.227(7) 1_554 5 ?
M1 M3 M2 121.227(7) . 5 ?
O3 M3 M2 90.0 5_556 . ?
O3 M3 M2 90.0 1_554 . ?
O1 M3 M2 138.993(19) 5 . ?
O1 M3 M2 138.993(19) 6 . ?
O1 M3 M2 41.007(19) 2 . ?
O1 M3 M2 41.006(19) . . ?
M1 M3 M2 121.227(6) 5 . ?
M1 M3 M2 121.227(7) 5_556 . ?
M1 M3 M2 58.773(7) 1_554 . ?
M1 M3 M2 58.773(7) . . ?
M2 M3 M2 180.0 5 . ?
O4 M4 O4 154.42(4) 8_455 7_556 ?
O4 M4 O2 81.63(3) 8_455 2_556 ?
O4 M4 O2 78.00(2) 7_556 2_556 ?
O4 M4 O2 78.00(3) 8_455 . ?
O4 M4 O2 81.63(3) 7_556 . ?
O2 M4 O2 74.02(3) 2_556 . ?
O4 M4 O6 141.63(3) 8_455 7_556 ?
O4 M4 O6 62.49(2) 7_556 7_556 ?
O2 M4 O6 135.31(2) 2_556 7_556 ?
O2 M4 O6 116.82(2) . 7_556 ?
O4 M4 O6 62.49(2) 8_455 8_455 ?
O4 M4 O6 141.63(3) 7_556 8_455 ?
O2 M4 O6 116.82(2) 2_556 8_455 ?
O2 M4 O6 135.31(2) . 8_455 ?
O6 M4 O6 86.62(3) 7_556 8_455 ?
O4 M4 O5 85.65(2) 8_455 7_556 ?
O4 M4 O5 108.70(2) 7_556 7_556 ?
O2 M4 O5 159.02(3) 2_556 7_556 ?
O2 M4 O5 87.09(2) . 7_556 ?
O6 M4 O5 61.68(2) 7_556 7_556 ?
O6 M4 O5 70.72(3) 8_455 7_556 ?
O4 M4 O5 108.70(2) 8_455 8_455 ?
O4 M4 O5 85.65(2) 7_556 8_455 ?
O2 M4 O5 87.09(2) 2_556 8_455 ?
O2 M4 O5 159.02(3) . 8_455 ?
O6 M4 O5 70.72(2) 7_556 8_455 ?
O6 M4 O5 61.68(2) 8_455 8_455 ?
O5 M4 O5 112.87(3) 7_556 8_455 ?
O4 M4 T2 171.57(2) 8_455 7_556 ?
O4 M4 T2 29.985(17) 7_556 7_556 ?
O2 M4 T2 105.772(17) 2_556 7_556 ?
O2 M4 T2 99.908(17) . 7_556 ?
```

```
O6 M4 T2 32.511(16) 7_556 7_556 ?
O6 M4 T2 116.03(2) 8_455 7_556 ?
O5 M4 T2 86.092(18) 7_556 7_556 ?
O5 M4 T2 76.163(18) 8_455 7_556 ?
O4 M4 T2 29.985(17) 8_455 8_455 ?
O4 M4 T2 171.57(2) 7_556 8_455 ?
O2 M4 T2 99.908(17) 2_556 8_455 ?
O2 M4 T2 105.772(17) . 8_455 ?
O6 M4 T2 116.03(2) 7_556 8_455 ?
O6 M4 T2 32.511(16) 8_455 8_455 ?
O5 M4 T2 76.163(18) 7_556 8_455 ?
O5 M4 T2 86.092(18) 8_455 8_455 ?
T2 M4 T2 147.73(2) 7_556 8_455 ?
O4 M4 M2 121.92(2) 8_455 . ?
O4 M4 M2 38.355(18) 7_556 . ?
O2 M4 M2 40.510(16) 2_556 . ?
O2 M4 M2 80.72(2) . . ?
O6 M4 M2 96.054(16) 7_556 . ?
O6 M4 M2 137.240(16) 8_455 . ?
O5 M4 M2 146.061(16) 7_556 . ?
O5 M4 M2 78.952(16) 8_455 . ?
T2 M4 M2 65.278(7) 7_556 . ?
T2 M4 M2 137.642(9) 8_455 . ?
O4 M4 M2 38.355(18) 8_455 1_556 ?
O4 M4 M2 121.92(2) 7_556 1_556 ?
O2 M4 M2 80.72(2) 2_556 1_556 ?
O2 M4 M2 40.510(16) . 1_556 ?
O6 M4 M2 137.241(16) 7_556 1_556 ?
O6 M4 M2 96.054(16) 8_455 1_556 ?
O5 M4 M2 78.952(16) 7_556 1_556 ?
O5 M4 M2 146.061(16) 8_455 1_556 ?
T2 M4 M2 137.642(8) 7_556 1_556 ?
T2 M4 M2 65.278(7) 8_455 1_556 ?
M2 M4 M2 109.520(18) . 1_556 ?
O1 T1 O7 111.49(4) . . ?
O1 T1 O6 110.93(4) . . ?
O7 T1 O6 109.16(5) . . ?
O1 T1 O5 112.93(4) . . ?
O7 T1 O5 105.40(5) . . ?
O6 T1 O5 106.64(4) . . ?
O1 T1 M3 34.23(2) . . ?
O7 T1 M3 78.71(4) . . ?
O6 T1 M3 134.04(3) . . ?
O5 T1 M3 114.79(3) . . ?
O1 T1 A2 131.81(3) . 7 ?
O7 T1 A2 48.51(5) . 7 ?
O6 T1 A2 117.08(3) . 7 ?
O5 T1 A2 57.05(4) . 7 ?
M3 T1 A2 102.051(19) . 7 ?
O1 T1 M1 33.11(2) . . ?
O7 T1 M1 114.70(4) . . ?
O6 T1 M1 79.49(3) . . ?
O5 T1 M1 134.88(3) . . ?
M3 T1 M1 57.477(7) . . ?
A2 T1 M1 158.28(3) 7 . ?
O1 T1 M2 34.06(2) . . ?
O7 T1 M2 134.37(4) . . ?
```

```
O6 T1 M2 112.02(3) . . ?
O5 T1 M2 80.85(3) . . ?
M3 T1 M2 58.730(8) . . ?
A2 T1 M2 121.786(15) 7 . ?
M1 T1 M2 56.606(7) . . ?
O1 T1 M4 129.37(3) . 7_556 ?
O7 T1 M4 119.13(4) . 7_556 ?
O6 T1 M4 53.18(3) . 7_556 ?
O5 T1 M4 53.46(3) . 7_556 ?
M3 T1 M4 159.532(10) . 7_556 ?
A2 T1 M4 85.30(3) 7 7_556 ?
M1 T1 M4 116.424(10) . 7_556 ?
M2 T1 M4 101.102(11) . 7_556 ?
O4 T2 O2 117.35(4) . . ?
O4 T2 O5 109.44(4) . 1_556 ?
O2 T2 O5 109.74(4) . 1_556 ?
O4 T2 O6 104.47(4) . . ?
O2 T2 O6 108.54(4) . . ?
O5 T2 O6 106.70(4) 1_556 . ?
O4 T2 M4 46.84(3) . 7_556 ?
O2 T2 M4 130.73(3) . 7_556 ?
O5 T2 M4 119.52(3) 1_556 7_556 ?
O6 T2 M4 57.64(3) . 7_556 ?
O4 T2 A2 115.68(3) . 7_556 ?
O2 T2 A2 126.88(3) . 7_556 ?
O5 T2 A2 52.98(3) 1_556 7_556 ?
O6 T2 A2 53.88(3) . 7_556 ?
M4 T2 A2 85.525(15) 7_556 7_556 ?
O4 T2 M4 80.50(3) . . ?
O2 T2 M4 37.48(2) . . ?
O5 T2 M4 133.48(3) 1_556 . ?
O6 T2 M4 114.64(3) . . ?
M4 T2 M4 100.633(8) 7_556 . ?
A2 T2 M4 161.10(2) 7_556 . ?
T1 O1 M1 120.77(4) . . ?
T1 O1 M3 119.02(4) . . ?
M1 O1 M3 97.51(3) . . ?
T1 O1 M2 119.91(4) . . ?
M1 O1 M2 95.40(3) . . ?
M3 O1 M2 99.04(3) . . ?
T2 O2 M1 123.28(4) . . ?
T2 O2 M2 123.56(4) . 1_556 ?
M1 O2 M2 94.18(3) . 1_556 ?
T2 O2 M4 118.36(3) . . ?
M1 O2 M4 99.02(3) . . ?
M2 O2 M4 91.20(3) 1_556 . ?
M3 O3 M1 96.31(3) 1_556 5_556 ?
M3 O3 M1 96.31(3) 1_556 . ?
M1 O3 M1 99.83(4) 5_556 . ?
M3 O3 H3 121.2(14) 1_556 . ?
M1 O3 H3 119.1(7) 5_556 . ?
M1 O3 H3 119.1(7) . . ?
T2 O4 M2 142.33(4) . 7_556 ?
T2 O4 M4 103.18(4) . 7_556 ?
M2 O4 M4 95.92(3) 7_556 7_556 ?
T2 O5 T1 133.65(5) 1_554 . ?
T2 O5 M4 122.25(4) 1_554 7_556 ?
```

```
T1 O5 M4 95.68(3) . 7_556 ?
T2 O5 A2 97.80(3) 1_554 7 ?
T1 O5 A2 91.48(4) . 7 ?
M4 O5 A2 110.75(3) 7_556 7 ?
T2 O6 T1 134.85(5) . . ?
T2 O6 M4 89.85(3) . 7_556 ?
T1 O6 M4 96.00(3) . 7_556 ?
T2 O6 A2 96.45(4) . 7_556 ?
T1 O6 A2 122.60(5) . 7_556 ?
M4 O6 A2 110.24(3) 7_556 7_556 ?
T1 O7 T1 132.97(7) 6 . ?
T1 O7 A2 100.91(5) 6 3_545 ?
T1 O7 A2 122.46(6) . 3_545 ?
T1 O7 A2 122.46(6) 6 7 ?
T1 O7 A2 100.91(5) . 7 ?
A2 O7 A2 21.85(8) 3_545 7 ?

_diffrn_measured_fraction_theta_max     0.955
_diffrn_reflns_theta_full               39.39
_diffrn_measured_fraction_theta_full    0.955
_refine_diff_density_max     1.001
_refine_diff_density_min    -1.020
_refine_diff_density_rms     0.099
```